ZEUS-prel-05-014

Submitted to the
XXXIII International Conference on High Energy Physics
July 26 - August 2, 2006, Moscow, Russia

Session: QCD hard interactions

Forward jets in deep inelastic scattering at HERA

ZEUS Collaboration

Abstract

Jet cross sections in neutral current deep inelastic scattering at low x_{Bj} and large pseudorapidity, towards the proton direction, have been measured with the ZEUS detector at HERA using an integrated luminosity of 81.8 pb^{-1}. Hadronic final-state measurements in this region are expected to be particularly sensitive to QCD evolution effects. In comparison to previous ZEUS measurements, the phase-space acceptance has been extended in pseudorapidity. The measurements have been compared with leading-logarithm parton-shower Monte Carlo models and next-to-leading-order QCD calculations

1 Introduction

In deep inelastic scattering (DIS) a parton in the proton can induce a QCD cascade consisting of several subsequent parton emissions before a quark absorbs the virtual photon. The scattered quark then radiates partons until hadronization sets in. Several different models of the QCD parton evolution dynamics have been proposed.

One set of parton evolution equations, derived on the basis of the collinear factorization theorem is that of Dokshitzer-Gribov-Lipatov-Altarelli-Parisi (DGLAP) evolution equations [1–3]. They are characterized by resummation of the terms of $\alpha_s \ln(Q^2)$. This approach assumes that the dominant contribution to the evolution comes from subsequent parton emissions which are strongly ordered in transverse momenta k_T. The parton with largest k_T corresponds to the parton interacting with the photon. DGLAP is applicable for the region $\ln(Q^2) \gg \ln(1/x)$, where x is the fraction of the proton's momentum belonging to the parton.

The Balitsky-Fadin-Kuraev-Lipatov (BFKL) [4] evolution equations allows the resummation of terms, independent of $\ln(Q^2)$. Therefore, the gluon ladder need not be ordered in k_T. The BFKL equations can be applied in the region $\ln(1/x) \gg \ln(Q^2)$ in the leading logarithmic approximation so that they are expected to primarily contribute to the evolution at low x.

The Ciafaloni-Catani-Fiorani-Marchesini (CCFM) [5,6] approach incorporates both types of evolution, DGLAP and BFKL, so that it should be applicable across the whole kinematic plane. They are based on the idea of coherent gluon radiation, which leads to angular ordering of gluon emissions in the gluon ladder such that $\theta_i > \theta_{i-1}$, where θ_i is the i-th gluon with respect to the incoming parton.

Differences between the above mentioned parton evolution dynamics are expected to be most prominent in the phase-space region towards the proton-remnant direction, i.e. away from the scattered quark. A forward jet is characterized by the fractional longitudinal momentum $x^{\rm jet} = p_z^{\rm jet}/p$, where p is the proton momentum and $p_z^{\rm jet}$ is the longitudinal jet momentum [7]. The transverse momentum is $k_T^{\rm jet}$.

This analysis includes jets measured in the forward region and focuses on the low x_{Bj} phase-space region which is expected to be better characterized by the BFKL parton evolution. To enhance the contribution of BFKL evolution, the events are required to satisfy:

- $(k_T^{\rm jet})^2 \sim Q^2$
- $x^{\rm jet} \gg x_{\rm Bj}$

The first condition suppresses the DGLAP evolution, leaving no room for strong ordering

in transverse momenta. The second condition demands that the jet carries a large fraction of the longitudinal momentum of the parent proton in order to maximize the phase space for the BFKL evolution.

The previous ZEUS publication on forward jet cross sections showed an enhancement of cross sections at low x_{Bj} beyond the DGLAP evolution in a range $\eta^{\mathrm{jet}} < 3$ [8]. Also H1 published similar results for $\eta^{\mathrm{jet}} < 2.7$ [9]. This paper investigates, with higher statistics, an extended pseudorapidity region (η^{jet} up to 3.5) and emphasizes the comparison of the measured cross sections with the CASCADE Monte Carlo (MC) [10] based on the CCFM evolution.

2 Experimental set-up

The analysis was performed with data taken with the ZEUS detector from 1998 to 2000, when HERA collided electrons or positrons[1] with energy of $E_e = 27.5\,\mathrm{GeV}$ with protons of energy $E_p = 920\,\mathrm{GeV}$ yielding a centre-of-mass energy of 318 GeV. The results are based on the sum of the e^-p and e^+p samples, corresponding to integrated luminosities of $16.4 \pm 0.3\,\mathrm{pb}^{-1}$ and $65.3 \pm 1.5\,\mathrm{pb}^{-1}$, respectively.

A detailed description of the ZEUS detector can be found elsewhere [11]. A brief outline of the components that are most relevant for this analysis is given below. Charged particles are tracked in the central tracking detector (CTD) [12], which operates in a magnetic field of 1.43 T provided by a thin superconducting solenoid. The CTD consists of 72 cylindrical drift chamber layers, organised in nine superlayers covering the polar-angle[2] region $15^\circ < \theta < 164^\circ$. The transverse-momentum resolution for full-length tracks is $\sigma(p_T)/p_T = 0.0058p_T \oplus 0.0065 \oplus 0.0014/p_T$, with p_T in GeV.

The high-resolution uranium–scintillator calorimeter (CAL) [13] consists of three parts: the forward (FCAL), the barrel (BCAL) and the rear (RCAL) calorimeters. Each part is subdivided transversely into towers and longitudinally into one electromagnetic section (EMC) and either one (in RCAL) or two (in BCAL and FCAL) hadronic sections (HAC). The smallest subdivision of the calorimeter is called a cell. The CAL energy resolutions, as measured under test-beam conditions, are $\sigma(E)/E = 0.18/\sqrt{E}$ for electrons and $\sigma(E)/E = 0.35/\sqrt{E}$ for hadrons, with E in GeV. The timing resolution of the CAL is better than 1 ns for energy deposits greater than 4.5 GeV.

[1] Hereafter, both e^+ and e^- are referred to as electrons, unless explicitly stated otherwise.

[2] The ZEUS coordinate system is a right-handed Cartesian system, with the Z axis pointing in the proton beam direction, referred to as the "forward direction", and the X axis pointing left towards the centre of HERA. The coordinate origin is at the nominal interaction point.

In 1998-2000, the forward plug calorimeter (FPC) [14] was installed in the 20×20 cm^2 beam hole of the FCAL, with a small hole of radius 3.15 cm in the center to accommodate the beam pipe. The FPC increased the forward calorimetric coverage by about 1 unit of pseudorapidity to $\eta \leq 5$. The FPC consisted of a lead–scintillator sandwich calorimeter divided longitudinally into electromagnetic and hadronic sections that were read out separately by wavelength-shifting fibers and photomultipliers. The energy resolution, as measured under test-beam conditions, was $\sigma(E)/E = 0.41/\sqrt{E} \oplus 0.062$ and $\sigma(E)/E = 0.65/\sqrt{E} \oplus 0.06$ for electrons and pions, respectively, with E in GeV. In order to assure the correct reconstruction of the jets near the boundary between FCAL and FPC, jet profiles have been simulated by MC and compared to data. No discrepancy has been observed.

3 Event and jet selection

The scattered electron was identified using an algorithm based on a neural network [15]. The kinematic variables Q^2 and $x_{\rm Bj}$ were reconstructed using the double-angle method (DA) [16] and y using $e\Sigma$ method [17] where the hadronic final state was reconstructed using combinations of CTD tracks and energy clusters measured in the CAL to form energy-flow objects (EFOs) [18].

The following criteria were applied offline to select DIS events:

- a scattered electron with energy above 10 GeV;
- the impact point of the scattered electron on the RCAL should lie outside the region 48×24 cm^2 centered on the beam line;
- $40 < \delta < 65$ GeV, where $\delta = \sum_i (E_i - P_{Z,i})$ and the sum runs over the EFOs from the hadronic system and the energy deposited by the identified electron;
- $0.04 < y_{e\Sigma} < 0.7$;
- a vertex position $|Z_{\rm vtx}| < 50$ cm;
- $20 < Q^2_{\rm DA} < 100\,{\rm GeV}^2$;
- $0.0004 < x_{\rm DA} < 0.005$.

The jet search was performed on all CAL and FPC cells, excluding those belonging to the scattered electron. The k_T cluster algorithm [19] in the longitudinally invariant inclusive mode [20] was applied in the Breit frame [21] to reconstruct jets in the hadronic final state both in data and in Monte Carlo (MC) simulated events. The reconstructed jets were then boosted to the laboratory frame and a jet energy correction was applied at the detector level in order to account for the energy loss of the hadrons in the inactive

material of the detector. The following jet selection cuts were applied in the laboratory frame:

- the transverse energy of the jets was selected to be $E_T^{\rm jet} > 5$ GeV, to ensure that the jets are well measured;
- the pseudorapidity of a jet was required to be $2 < \eta^{\rm jet} < 3.5$. In this angular region of the detector acceptance the selected forward jets are reasonably well reconstructed;
- the scaled longitudinal momentum was required to satisfy $x_{\rm jet} > 0.036$, which selected forward jets with a large energy;
- the cut $0.5 < (E_T^{\rm jet})^2/Q^2 < 2$ selected the phase space region where BFKL effects are expected to be dominant and DGLAP effects are suppressed.

4 Results and Conclusion

In the following cross sections are presented as functions of the variables Q^2, $x_{\rm Bj}$, $E_T^{\rm jet}$ and $\eta^{\rm jet}$. The differential jet cross sections for any given variable ξ in the kinematic region $20 < Q^2 < 100\,{\rm GeV}^2$, $0.04 < y < 0.7$ and $0.0004 < x_{\rm Bj} < 0.005$ were determined using:

$$\frac{d\sigma}{d\xi} = \frac{N^{\rm jet}}{A\ \mathcal{L}\ \Delta\xi},$$

where $N^{\rm jet}$ is the number of jets in a bin of width $\Delta\xi$, A is the acceptance for that bin, and $\mathcal{L}$ is the integrated luminosity. The acceptance correction factors were obtained from the ARIADNE 4.08 [22] MC and the LEPTO 6.5.1 [23] MC programs interfaced to HERACLES 4.6.1 [24] via DJANGO 1.1 [25]. The average between the correction values obtained with ARIADNE and LEPTO MC was used to correct the data to the hadron level.

The major sources of the systematic uncertainty were as the follows, where the effects on the cross sections are shown in parentheses:

- the largest uncertainty was obtained from the model dependence of the detector corrections. This uncertainty has been estimated using the deviations of LEPTO and ARIADNE corrections from their average ($\leq 15\%$);
- a shift of $\pm$ 3% due to the CAL energy-scale uncertainty (< 10 %);
- the selection of inclusive DIS events ($< 1\%$). Variations were made for the scattered-electron energy cut, the RCAL box cut, the δ cut and the vertex-position cut;
- a shift of $\pm$ 10% due to the FPC energy-scale uncertainty ($\sim 5\%$ for the last $\eta^{\rm jet}$ bin; everywhere negligibe).

These systematic uncertainties were added in quadrature separately for the positive and negative variations in each bin in which the differential cross sections were measured.

Figure 1 compares the measured cross sections as function of Q^2, $x_{\rm Bj}$, $E_T^{\rm jet}$ and $\eta^{\rm jet}$ with the predictions of different MC models. The ARIADNE MC is based on the BFKL-like Color Dipole Model (CDM) [26–28] which produces a cascade of gluons not strongly ordered in k_T. LEPTO MC is a pure DGLAP type MC based on the first-order QCD matrix elements plus parton showers (MEPS). For the generation of the LEPTO sample, the soft-color interactions have been witched off [29]. The CASCADE MC [10, 30] based on CCFM parton evolution uses k_T-factorization of the cross section into an off-shell matrix element and an unintegrated gluon density function. The following sets of CCFM unintegrated gluon density function have been tried for comparison with data: J2003 set 1 and J2003 set 2 [31]. The latter version includes non-singular terms in the splitting function and lowers the cross sections at low $x_{\rm Bj}$. ARIADNE and LEPTO have QED corrections included, while CASCADE has not, however the effect of the QED radiation is expected to be small [8]. In all MC models fragmentation has been performed using the LUND [32] string model as implemented in JETSET 7.4 [33].

The predictions of ARIADNE reproduce the shapes and the normalizations of the differential cross sections. LEPTO describes well the shapes of the data but is lower than the data by a factor of two. CASCADE with J2003 set 2 describes the integrated cross sections better than J2003 set 1. However it does not reproduce the shapes of the distributions in $x_{\rm Bj}$ and $\eta^{\rm jet}$.

Figure 2 compares the measurements with the predictions of next-to-leading-order QCD calculations as it is implemented in DISENT program. The DISENT [34], using current parameterizations of the proton PDFs based on DGLAP evolution, allows calculations that sum up to two orders of the perturbation series. The calculations were performed in the $\overline{\rm MS}$ renormalization and factorization schemes. The number of flavors was set to five; the renormalization (μ_R) and factorization (μ_F) scales were both set to $\mu_R = \mu_F = Q$. The CTEQ5D [35] parameterization of the proton PDF were used. The uncertainty in the calculations was estimated by varying μ_R by a factor of two up and down. The effect on the calculations is up to 50%, depending on the phase-space region. Hadronisation effects are not included in the DISENT program. Therefore, samples of Monte Carlo events were generated to correct the QCD calculations for hadronisation effects. The uncertainty on the hadronisation correction was taken to be the absolute difference in the correction factors obtained with ARIADNE and LEPTO MC programs.

The NLO calculations describe the measurement within theoretical uncertainties. The variation of the calculations with the renormalization scale is large, emphasizing the need for higher-order calculations.

In conclusion, a new measurement of the jet cross sections has been performed in the forward region, $2 < \eta^{\rm jet} < 3.5$, with higher statistics and smaller systematic errors than the previous publications mentioned above. The ARIADNE MC model gives the best overall description of the cross sections, CASCADE reproduces integrated cross sections, but fails to describe the shapes of the differential cross sections in $x_{\rm Bj}$ and $\eta^{\rm jet}$. These experimental results may be used to adjust the parameters of the intrinsic k_T distribution. The NLO calculations are lower than data but within theoretical uncertainties. However, a large renormalization uncertainty does not permit a more detailed comparison.

References

[1] V.N. Gribov and L.N. Lipatov, Sov. J. Nucl. Phys. **15**, 438 (1972).

[2] Yu.L. Dokshitzer, Sov. Phys. JETP **46**, 641 (1977).

[3] G. Altarelli and G. Parisi, Nucl. Phys. **B 126**, 298 (1977).

[4] Ya.Ya. Balitskiĭ and L.N. Lipatov, Sov. J. Nucl. Phys. **28**, 822 (1978).

[5] M. Ciafaloni, Nucl. Phys. **B 296**, 49 (1988).

[6] S. Catani, F. Fiorani and G. Marchesini, Nucl. Phys. **B 336**, 18 (1990).

[7] A.H. Mueller, Nucl. Phys. Proc. Suppl. **18 C**, 125 (1991).

[8] ZEUS Coll., S. Chekanov et al., Report DESY-05-117, DESY, 2005.

[9] H1 Coll., C. Adloff et al., Nucl. Phys. **B 538**, 3 (1999).

[10] H. Jung and G. P. Salam, Eur. Phys. J. **C 19** (2001).

[11] ZEUS Coll., U. Holm (ed.), *The ZEUS Detector*. Status Report (unpublished), DESY (1993), available on `http://www-zeus.desy.de/bluebook/bluebook.html`.

[12] N. Harnew et al., Nucl. Inst. Meth. **A 279**, 290 (1989);
B. Foster et al., Nucl. Phys. Proc. Suppl. **B 32**, 181 (1993);
B. Foster et al., Nucl. Inst. Meth. **A 338**, 254 (1994).

[13] M. Derrick et al., Nucl. Inst. Meth. **A 309**, 77 (1991);
A. Andresen et al., Nucl. Inst. Meth. **A 309**, 101 (1991);
A. Caldwell et al., Nucl. Inst. Meth. **A 321**, 356 (1992);
A. Bernstein et al., Nucl. Inst. Meth. **A 336**, 23 (1993).

[14] A. Bamberger et al., Nucl. Inst. Meth. **A 450**, 235 (2000).

[15] H. Abramowicz, A. Caldwell and R. Sinkus, Nucl. Inst. Meth. **A 365**, 508 (1995);
R. Sinkus and T. Voss, Nucl. Inst. Meth. **A 391**, 360 (1997).

[16] S. Bentvelsen, J. Engelen and P. Kooijman, *Proc. Workshop on Physics at HERA*, W. Buchmüller and G. Ingelman (eds.), Vol. 1, p. 23. Hamburg, Germany, DESY (1992);
K.C. Höger, *Proc. Workshop on Physics at HERA*, W. Buchmüller and G. Ingelman (eds.), Vol. 1, p. 43. Hamburg, Germany, DESY (1992).

[17] U. Bassler and G. Bernardi, Nucl. Inst. Meth. **A 426**, 583 (1999).

[18] ZEUS Coll., J. Breitweg et al., Eur. Phys. J. **C 1**, 81 (1998).

[19] S.Catani et al., Nucl. Phys. **B406**, 187 (1993).

[20] S.D. Ellis and D.E. Soper, Phys. Rev. **D 48**, 3160 (1993).

[21] K.H. Streng, T.F. Walsh, P.M. Zerwas, Z. Phys. **C**, 237 (1979).

[22] L. Lönnblad, Comp. Phys. Comm. **71**, 15 (1992).

[23] G. Ingelman, A. Edin and J. Rathsman, Comp. Phys. Comm. **101**, 108 (1997).

[24] A. Kwiatkowski, H. Spiesberger and H.-J. Möhring, Comp. Phys. Comm. **69**, 155 (1992). Also in *Proc. Workshop Physics at HERA*, 1991, DESY, Hamburg.

[25] K. Charchula, G.A. Schuler and H. Spiesberger, Comp. Phys. Comm. **81**, 381 (1994).

[26] G. Gustafson, Phys. Lett. **B 175**, 453 (1986).

[27] Gösta Gustafson and Ulf Petterson, Nucl. Phys. **B 306**, 746 (1988).

[28] B. Andersson, G. Gustafson, L. Lönnblad, U. Petterson, Z. Phys. **C 43**, 625 (1989).

[29] ZEUS Coll., J. Breitweg et al., Eur. Phys. J. **C 11**, 251 (1999).

[30] H. Jung, Comp. Phys. Comm. **143**, 100 (2002).

[31] M. Hansson, H. Jung, The status of CCFM unintegrated gluon densities in *DIS 2003, XI International Workshop on Deep Inelastic Scattering, St. Petersburg, Russia.* (2003). Also in preprint hep-ph/0309009.

[32] B. Andersson et al., Phys. Rep. **97**, 31 (1983).

[33] T. Sjöstrand, Comp. Phys. Comm. **82**, 74 (1994).

[34] S. Catani and M.H. Seymour, Nucl. Phys. **B 485**, 579 (1998).

[35] CTEQ Coll., H.L. Lai et al., Eur. Phys. J. **C 12**, 375 (2000).

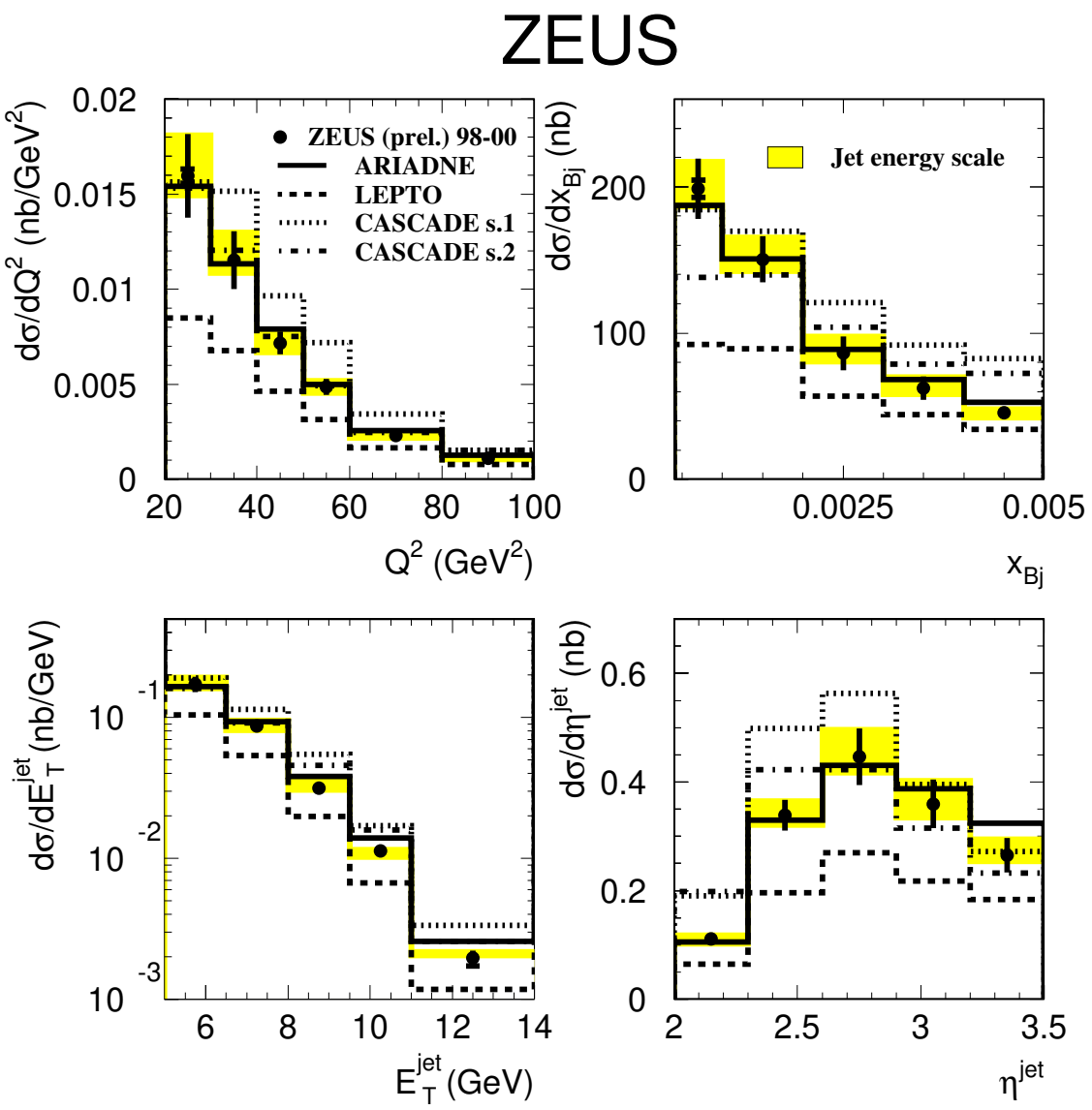

Figure 1: *Differential cross sections for inclusive jet production for the data (dots) compared with the ARIADNE (solid histogram), LEPTO (dashed histogram) and CASCADE (dotted and point-dashed histograms) predictions. The shaded area shows the uncertainty after varying the CAL energy scale in MC of ±3 % . The cross sections are shown as a function of Q^2, x_{Bj}, $E_{T,jet}$, and η^{jet}. The inner error bars indicate the statistical uncertainties, while the outer ones correspond to statistical and systematic uncertainties (except the CAL energy-scale uncertainty) added in quadrature.*

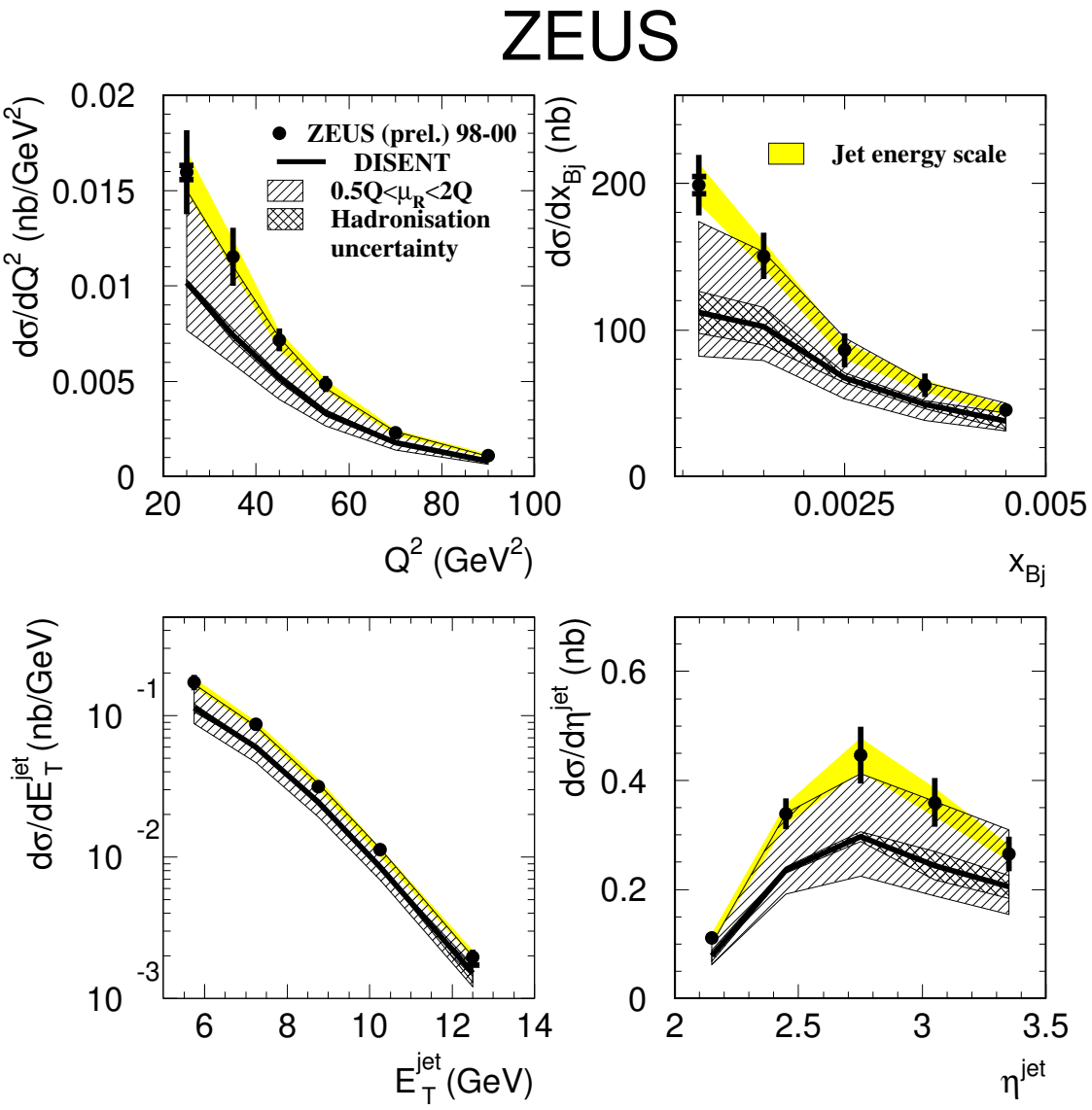

Figure 2: *Differential cross sections for inclusive jet production for the data (dots) compared with the NLO QCD calculations (solid line). The hatched area shows the theoretical uncertainities and the shaded area shows the uncertainty after varying the CAL energy scale in MC ±3 % . The cross sections are shown as a function of Q^2, x_{bj}, $E_{T,jet}$, and η_{jet}. The inner error bars indicate the statistical uncertainties, while the outer ones correspond to statistical and systematic uncertainties (except the CAL energy-scale uncertainty) added in quadrature.*